Chromium doped tungsten alloy for plasma-facing components of fusion reactors formed by compression plasma flows

Chromium doped tungsten alloy for plasma-facing components of fusion reactors formed by compression plasma flows

S Al Mazrouei[1, *], A Mohanta[1, *], V I Shymanski[2], G Matras[1] and C Kasmi[1]

[1] Directed Energy Research Center, Technology Innovation Institute, Abu Dhabi, UAE
[2] Belarusians State University, Minsk, Belarus

*E-mail: shamma.almazrouei@tii.ae, antaryami.mohanta@tii.ae

Abstract. Chromium doped tungsten (Cr-W) alloys are formed by compression plasma flows (CPFs) treatment at different absorbed energy densities (20 – 50 J/cm^2), and are characterized by X-ray diffraction (XRD), scanning electron microscopy (SEM), energy dispersive X-ray microanalysis (EDX), and the Vickers hardness test. XRD analysis betokens that the dominant crystal orientation changes from (110) to (200) after CPFs treatment, and the intensity ratio (I_{200}/I_{110}) between the diffraction lines corresponding to (200) and (110) planes increases with an increase in the absorbed energy density. SEM and EDX analyses betoken spatial inhomogeneity at 20 J/cm^2, improved uniformity at 30 J/cm^2, and cracks at higher energy density. The hardness of the Cr–W alloy varies with absorbed energy density and has a maximum value of 379 HV at 20 J/cm^2.

1. Introduction

Tungsten is considered as the main candidate for the plasma-facing components (PFCs) in future nuclear fusion reactors (ITER and DEMO) due to its high melting point, low hydrogen isotopes retention, and high resistance to sputtering [1]. However, its acute brittleness, low formability, and high brittle to ductile transition temperature (BDTT) can cause radiation damage that further results in dislocation loops and other defective structures such as self-interstitial atoms (SIAs), voids, cracks, etc. [2]. Surface cracking and subsequent erosion from the tungsten surface can contaminate the plasma and retard the reaction in the fusion reactor [3]. In addition, the high heat loads and high fluencies of neutron and ion irradiation, such as helium and hydrogen on tungsten lead to bubble formation, flecking, and blistering [4, 5]. The use of pure W in a fusion reactor could result in radioactive and highly volatile WO_3 compounds [6]. Oxidation of W can be suppressed, and hardness can be improved by alloying with chromium (Cr) [2,6]. Oxidation of Cr to form Cr_2O_3 is more favourable than that of W to result in WO_3 as the Gibbs free energy (ΔG) for the formation of Cr_2O_3 is more negative than that of WO_3 indicating the preferable formation and enhanced stability of Cr_2O_3 in Cr-W alloy [7]. The formed Cr_2O_3 layer is stable up to 1400 ^{o}C which indicates that it can act as a protective layer for W in Cr-W alloy and make the material extremely resistant to the environmental corrosion. High melting point (1863 ^{o}C) and high strength-to-density ratio of Cr make Cr-W alloy a good candidate for plasma facing components [8]. Furthermore, the Cr-W phase diagram reveals Cr-W alloy as isomorphic structure with a miscibility gap below 1677 ^{o}C [7, 9]. Moreover, the ΔG for Al_2O_3 is -1582.3 kJ/mol which is even more negative than that of Cr_2O_3 i.e., ΔG = - 1049.96 kJ/mol [10]. Thus, alloying of W with Al can be considered for PFCs. However, melting point (m_p) of Al is much less than that of chromium, i.e., m_p = 660.3 ^{o}C and 1907 ^{o}C of Al and Cr, respectively. This indicates that the low melting point of Al can encumber the high-temperature performance of the Al-W alloy. Therefore, Cr-W alloy is superior to Al-W alloy for high-temperature applications and PFCs. Heating, melting and casting-based techniques or the powder technologies are not convenient for the production of Cr-W alloy due to the high melting temperature of tungsten. Low melting point sintering activators such as palladium (pd) has been

used to prepare Cr-W alloys by powder sintering since the inter-diffusion in Cr-W alloys is known to be very slow. Furthermore, high-energy mechanical milling to fabricate the Cr-W alloy has certain drawbacks, such as more energy consumption due to long milling time and introduction of contamination from the milling media. Liu *et al.* [11] have used combustion synthesis technique to prepare W-Cr alloy and achieved about 50% higher hardness than that of W-Cr alloys prepared by conventional powder sintering. So, the described methods of the tungsten-based alloys formation require high temperature techniques and are ineffective due to high difference in the melting points of the tungsten and the dopants. During the melt mixing, the low-temperature component will evaporate very fast, and it is very difficult to obtain required concentrations in the alloys. In our experiments we propose to use quasi-stationary plasma accelerators for material melting in the pulsed mode. This method of materials modification is based on the fast energy transformation from the plasma flow to the surface layer of the target. The energy transformation occurs during the relatively small time (some tens or hundreds of μs). The combination of high energy density and small time of the process allows to produce solid state from the melted state in the non-equilibrium conditions. This compression plasma flows (CPFs) treatment has already been employed for the surface modification and surface layer alloying, which involves melting of the surface layer and the subsequent mixing of materials in liquid phase [5,12]. In this study, we have prepared the Cr-W alloys by CPFs treatment on the Cr coated tungsten surface, which are characterized by X-ray diffraction (XRD), scanning electron microscopy (SEM), energy dispersive X-ray microanalysis (EDX), and the Vickers hardness test. The plasma treatment results in the melting and subsequent modification of the tungsten material, which leads to the maximum hardness of 379 HV.

2. Experimental

Figure 1(a) shows the schematics of the CPFs treatment set up. CPFs are the intense pulsed plasma flows produced by a magnetoplasma compressor of compact geometry. The chamber was filled with nitrogen gas (N_2) with constant voltage of 4 kV between the electrodes. The length (L) of CPFs from the edge of the electrode shown in figure 1(a) was 8 – 12 cm. The plasma velocity in CPFs ranges from 3×10^6 to 7×10^6 cm/s and the electron temperature was between 2 and 4 eV. The compression region starts to form near the edge of the electrodes. The compression plasma flow discharge duration was 100 μs which becomes stable around 80 μs.

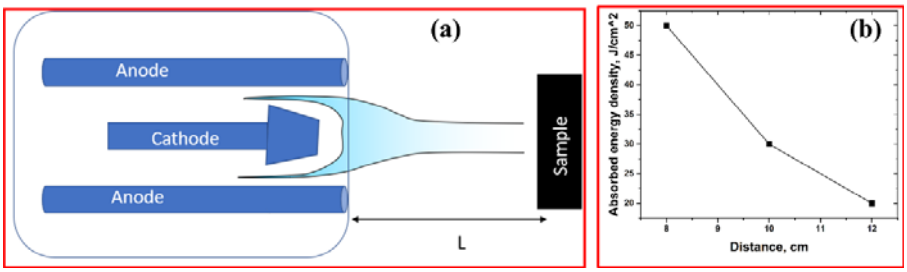

Figure 1. (a) Schematic representation of the sample treatment process by CPFs. (b) Variation of the absorbed energy density in the tungsten with distance (L) after CPFs treatment.

The samples were placed vertically with respect to the axis of CPFs at different distances (L) from the electrode edge. The modification of structural and phase composition of the materials by CPFs treatment has been attributed to the transfer of the absorbed energy density (Q) into heat, and the values of the absorbed energy densities were obtained similar to the previous report [4]. The highest absorbed energy density has the value of 50 J/cm^2 at L= 8 cm and decreases to 20 J/cm^2 at L= 12 cm as shown in figure 1(b). Each sample was exposed to three pulses with a time interval of 20 – 30 s.

A thin layer of chromium with thickness of 1 μm was coated on the surface of tungsten with thickness of 2 mm by vacuum-arc deposition, where this technique involves the initiation of an arc by contacting a cathode made of a target material. The cathode vapor plasma produced from high current discharge in vacuum and transported to a tungsten substrate to deposit coating of chromium on the surface. Chromium coated tungsten samples were subjected to the CPFs treatment. The structural and morphological characterizations of the samples were performed. The surface morphology of the samples was investigated by scanning-electron microscopy (SEM) using LEO 1455 VP microscope. By using the energy-dispersion X-ray microanalysis (EDX), the elemental composition was determined. For phase analysis, X-ray diffraction (XRD) was carried out by an Ultima IV RIGAKU diffractometer with X-ray wavelength of λ = 0.15418 nm. Vickers hardness test was conducted to determine hardness by using MVD 402 Wolpert Wilson Instrument. The diamond tip penetration depth was 1.7 μm.

3. Results and discussion

Figure 2 shows the XRD spectrum of the pure tungsten in the initial state without CPFs treatment which shows clear diffraction peaks corresponding to the (110), (200), (211) and (220) planes. The most dominant crystal orientation is along (110) diffraction line. The degree of crystal orientation for each diffraction peak is determined by the Lotgering's relation [13, 14] $D_{hkl} = I(hkl)/\Sigma I(hkl)$, where D_{hkl} is the degree of crystal orientation along the [hkl] direction, I(hkl) is the intensity of the corresponding (hkl) diffraction peak, and $\Sigma I(hkl)$ is the sum of the intensities of all the diffraction peaks having miller indices (hkl). The degree of crystal orientation is therefore obtained as 0.38, 0.33, 0.26 and 0.03 corresponding to (110), (200), (211) and (220) plane of pure tungsten, respectively. The interplanar distance d_{hkl} is determined by using the Bragg's diffraction condition: $2d_{hkl} \sin\theta = n\lambda$, where n is the diffraction order, which is 1 for the first order, and θ is the Bragg angle. The values of the interplanar spacing, d_{hkl} and the degree of crystal orientation, D_{hkl} for pure tungsten obtained from the XRD analysis are listed in table 1.

Table 1. List of d_{hkl} and D_{hkl} for pure tungsten.

No	2θ (degree)	θ (degree)	Sinθ	d_{hkl} (nm)	(hkl)	D_{hkl}
1	40.35	20.18	0.3448	0.2235	W (110)	0.38
2	58.36	29.18	0.4875	0.1581	W (2 0 0)	0.33
3	73.29	36.65	0.5968	0.1291	W (2 1 1)	0.26
4	87.09	43.55	0.6988	0.1189	W (2 2 0)	0.03

After the CPFs treatment, the change in structure of the surface layer of the material is expected due to the heat produced by plasma flows. Moreover, the temperature of the surface increases as the absorbed energy density increases from 20 to 50 J/cm^2 and thus increase in the melted layer depth. The phase analysis of the chromium coated tungsten treated by compression plasma flows was investigated by XRD. Figure 3 shows the XRD spectra of CPFs treated tungsten at different absorbed energy densities from 20 to 50 J/cm^2. The dominant crystal orientation changed from (110) to (200) due to the CPFs treatment indicating the change in crystal structure. The degree of crystal orientation along (200), i.e., D_{200} is 0.4, 0.5 and 0.8 for the Cr coated tungsten samples after CPFs treatment at different absorbed energy densities 20, 30 and 50 J/cm^2, respectively. This indicates that the increase in absorbed energy density from 20 to 50 J/cm^2 results in the transition from polycrystalline to single crystalline structure of the samples. Careful analysis reveals that the samples at 20 J/cm^2 comprises both the phases of chromium and tungsten which could be attributed to inappropriate liquid phase mixing due to reduced melt layer depth caused by insufficient absorbed energy density. At higher absorbed energy densities of 30 J/cm^2 and 50 J/cm^2, only single phase of W is observed in the XRD spectra (Figure 3), which indicates the formation of solid solution caused by appropriate liquid

phase mixing due to increasing melt layer depth under the increasing influence of compression plasma flows.

Once the plasma flows stop, the crystallization process starts. The melted tungsten crystallizes with a high cooling rate, which changes the grain structure of the sub-surface solidified layer. Moreover, the high cooling rate provides a high level of internal mechanical stress, i.e., tensile stress.

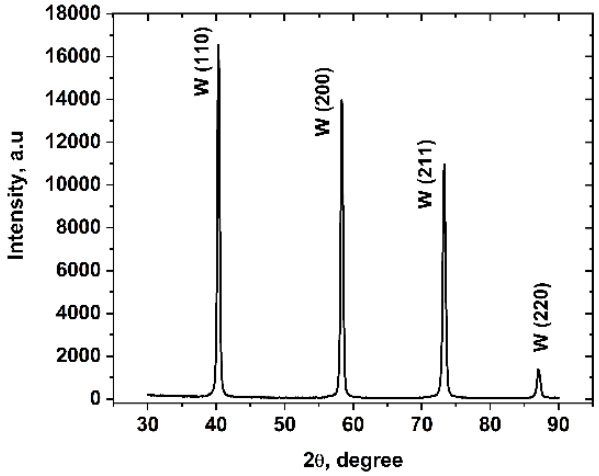

Figure 2. XRD pattern of the pure tungsten in initial state without CPFs treatment.

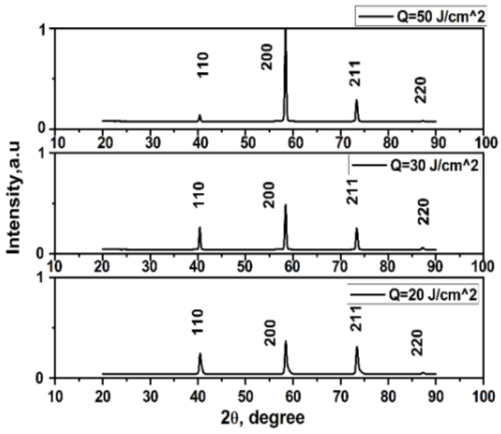

Figure 3. XRD patterns of the chromium coated tungsten after CPFs treatment at different absorbed energy densities (20 – 50 J/cm^2).

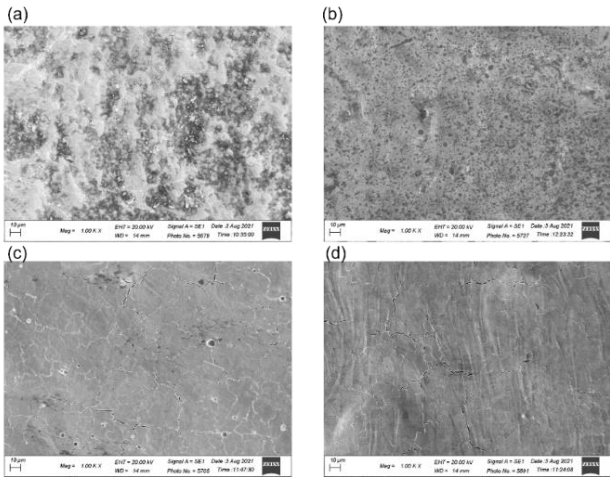

Figure 4. SEM images of the surface of pure tungsten (a) and W-Cr alloys formed after CPFs treatment with absorbed energy density of 20 J/cm^2 (b), 30 J/cm^2 (c), and 50 J/cm^2 (d).

Figure 4 shows the SEM imagery of the surface of pure tungsten (a) and W-Cr alloys formed after CPFs treatment with absorbed energy density of 20 J/cm^2 (b), 30 J/cm^2 (c), and 50 J/cm^2 (d). SEM shows the contrast mode of chromium formation on the tungsten substrate. As the absorbed energy density increases, the surface topography changes. The pure tungsten has a lot of holes because of plate rolling to have a

specific shape of metal sheet. At absorbed energy density of 20 J/cm^2, the surface morphology shows spatial inhomogeneity, which further depicts improved uniformity at absorbed energy density of 30 J/cm^2. At absorbed energy density of 50 J/cm^2, SEM imagery reveals formation of cracks. Furthermore, the average percentage of chromium is found to be about 32 wt.%, 0.3 wt.% and 0.1 wt.% from the EDX analysis at absorbed energy density of 20, 30 and 50 J/cm^2, respectively. This indicates that more chromium remains near the surface due to the reduced melt layer depth caused by insufficient absorbed energy density at 20 J/cm^2. Above 30 J/cm^2, melt layer depth increases which results in penetration of more chromium atoms into the bulk of the tungsten that leads to reduction in chromium percentage near the surface.

The alloying of the tungsten with chromium atoms after the CPF impact provides the W(Cr) solid formation at appropriate conditions. The dissolution of chromium atoms in the tungsten crystal lattice causes the internal mechanical stress and local deformations due to difference in the atomic radii. The change in the internal structure of the tungsten can play an important role when heating the samples at elevated temperatures. Indeed, during heating the oxygen diffusion results in oxide layer growth and deteriorates the performance of tungsten. However, the internal mechanical stress can cause the motion of oxygen atoms in the opposite direction, which reduces the diffusion process. So, it can positively influence on corrosion resistance of tungsten. The earlier results showed the increase in the structural stability under heating in air atmosphere after CPF treatment [15].

Modification of the structure and phase composition of the tungsten by alloying it with chromium leads to the change in the mechanical properties of the surface. The hardness shows how the material is resistant to plastic deformation because of the dislocation motion in the material. The samples treated by CPFs at absorbed energy density of 20 J/cm^2 has the highest hardness of 379 HV.

4. Conclusions

Compression plasma flows (CPFs) treatment was used to form chromium doped tungsten (Cr–W) alloys at different absorbed energy densities (20 – 50 J/cm^2). The impact of intense pulsed compression plasma flows on the chromium coated tungsten surface melts the surface layer and modify the surface properties. The increase in melt layer depth with increase in the absorbed energy density from 20 to 50 J/cm^2 increases the incorporation of more chromium atoms into the tungsten matrix. XRD analysis reveals that the dominant crystal orientation changes from (110) to (200) after CPFs treatment, and the intensity ratio (I_{200}/I_{110}) between the diffraction lines corresponding to (200) and (110) planes increases with an increase in the energy density. The increase in degree of crystal orientation along (110) plane with increase in absorbed energy density from 20 to 50 J/cm^2 indicates the transition from polycrystalline to single crystalline nature of the sample. SEM and EDX analyses betoken spatial inhomogeneity at 20 J/cm^2, improved uniformity at 30 J/cm^2, and cracks at higher energy density. The hardness of the Cr-W alloy varies with energy density and has a maximum value of 379 HV at 20 J/cm^2. The results indicate that the compression plasma flows treatment can be an effective technique for surface alloying in metals with large value of hardness.

Acknowledgments

The author would like to give her most sincere thanks to Dr. V. I. Shymanski, Dr. A. Mohanta, Dr. N. Mora and Dr. C. Kasmi for supervising the project. S. Al Mazrouei and A. Mohanta contributed equally.

References

[1] Hasegawa A, Fukuda M, Nogami S and Yabuuchi K 2014 Neutron irradiation effects on tungsten materials *Fusion Eng. Design* **89**(7–8) 1568–72.

[2] Ferroni F, Yi X, Arakawa K, Fitzgerald S P, Edmondson P D and Roberts S G 2015 High temperature annealing of ion irradiated tungsten *Acta Materialia* **14**(90) 380-393.
[3] Ibano K, Tsutsui T, Lang T, Togo S and Ogawa Y 2015 Effects of impurity transport and melt layer motion to the tungsten wall erosion during anomaly events *J. Nuclear Mater.* **4(**463) 185-188.
[4] Shymanski V I, Uglov V, Cherenda N, Pigasova V, Astashynski V, Kuzmitski A, Remnev G 2019 Structure and phase composition of tungsten alloys modified by compression plasma flows and high-intense pulsed ion beam impacts *Appl. Surf. Sci.* **10**(491) 43-52
[5] Uglov V, Anishchik V, Cherenda N, Stalmashonak A, Astashinski V, Kuzmickii A, Kovyazo A 2005 Mixing of chromium/carbon steel by compressive plasma flows *Vacuum* **78**(2-4) 489-493.
[6] Pitts R, Carpentier S, Escourbiac F, Hirai T, Komarov V, Lisgo S, Stangeby P 2013 A full tungsten divertor for ITER: Physics issues and design status *J. Nuclear Mater.* **9(**438)
[7] Telu S, Patra A, Sankaranarayana M, Mitra R and Pabi S 2013 Microstructure and cyclic oxidation behavior of W–Cr alloys prepared by sintering of mechanically alloyed nanocrystalline powders. *Int. J. Refract. Met. H.* **13**(36) 191-203
[8] Terentyev D, Khvan T, You J and Van Steenberge N 2020 Development of Chromium and chromium-tungsten alloy for the plasma facing components: Application of vacuum arc melting techniques *J. Nuclear Mater.* **11**(536) 152204
[9] Calvo A, García-Rosales C, Koch F, Ordás N, Iturriza I, Greuner H, Sarbu C 2016 Manufacturing and testing of self-passivating tungsten alloys of different composition *Nuclear Materials and Energy* **9** 422-429.
[10] Ziemniak S E, Anovitz L M, Castelli R A and Porter W D 2007 Thermodynamics of Cr_2O_3, $FeCr_2O_4$,$ZnCr_2O_4$, and $COCr_2O_4$ *J. Chemical Thermodynamics* **39**(11) 1474-1492.
[11] Dingdong F, Li J, Chen K, He G, Yang Z and Guo S 2016 Combustion synthesis of W–CR alloys with hierarchical microstructure and improved hardness *Mater. Lett.,* **3(**166) 43-45.
[12] Shymanski V I, Jevdokimovs A, Cherenda N N, Astashynski V M and Petrikova E A 2021 Structure and phase composition of hypereutectic silumin alloy al – 20si after compression plasma flows impact. *Journal of the Belarusian State University* (2) 25-33.
[13] Mohanta A and Thareja R K 2008 Photoluminescence study of ZnO nanowires grown by thermal evaporation on pulsed laser deposited Zno buffer layer *J. Appl. Phys.* **104**(4) 044906.
[14] Lotgering F 1959 Topotactical reactions with ferrimagnetic oxides having hexagonal crystal structures—I *J. Inorg. Nuclear Chem.* **9**(2) 113-123.
[15] Shymanski V I, Cherenda N N, Uglov V V, Astashynski V M and Kuzmitski A M 2018 Thermal stability of the structure and phase composition of titanium treated with compression plasma flows. *J. Surf. Invest. X-ray, Synchrotron and Neutron Techniques* **12**(4) 710-716.